JOURNAL OF AERONAUTICAL MATERIALS
ISSN: 1005-5053
Vol. 44, Issue-01, 2024
pp. 270-279

INVESTIGATION OF RETRO-PROPULSION-BASED FLOW FIELD AROUND RE-ENTRY CREW MODULES

Rinchu P.[1], Anaagh K.[2], Hridya Nambiar[3], Sayanth R.[4], Vishnu Sankar V.[5]
[1] Assistant Professor, Department Of Aeronautical Engineering, Jawaharlal College Of Engineering And Technology [2],[3],[4],[5] Final Year B.tech Students, Jawaharlal College Of Engineering And Technology

Abstract—Crew modules intended for re-entry are intricately designed with blunt shapes to endure the intense heat flux experienced during this phase. This research concentrated on bow shock formation around the blunt body during rapid hypersonic flow, providing insight into the resultant aerodynamic heating. CFD was utilized to simulate high-speed hypersonic flows over the Orion CEV. The focus was on analyzing the effects of retro-propulsion systems, specifically considering two nozzle exhaust conditions: Mach numbers 2 and 4. By modeling the airflow around the re- entry module, simulations were conducted to evaluate the reduction in heat flux achieved with varying nozzle exhaust conditions. It was analyzed that the Mach 4 nozzle exhaust condition proved more efficient in decreasing heat flux by redirecting the bow shock wave away from the crew module body compared to the Mach 2 nozzle exhaust condition. The analysis encompassed assessments of velocity, temperature, heat flux, and pressure distributions. Comparisons were conducted between crew modules re-entering without retro- propulsion systems, offering valuable insights into the effectiveness of such systems in reducing heat flux during re- entry.
Keywords—CEV, Hypersonic, Heat flux, Retro- propulsion, Nozzle

aerodynamic problems. One of the main problems associated with re-entry vehicles is aerodynamic heating after re-entry into the earth's atmosphere [1].
To mitigate aerodynamic heating in the Crew Exploration Vehicle (CEV), a variety of methods are introduced. Thermal Protection Systems (TPS) are employed [2], incorporating advanced materials like ablative heat shields, ceramic tiles, or thermal blankets to absorb and dissipate heat during re-entry. One potential disadvantage of the TPS is the need for regular maintenance and inspection due to wear, degradation, and potential vulnerabilities to impact damage. Active cooling systems circulate coolants or utilize heat exchangers to remove heat from critical components during high-speed flight. Passive cooling techniques like thermal coatings or radiative cooling surfaces help dissipate heat and lower overall temperatures.

1. INTRODUCTION

Re-entry denotes the process whereby a spacecraft re-enters Earth's atmosphere. The Crew Exploration Vehicle (CEV) is designed to ferry human astronauts to destinations like the International Space Station and the moon, then safely bring them back to Earth. The thick layer of gas enveloping our planet serves as a valuable mechanism for deceleration due to aerodynamic drag. Human space exploration has witnessed significant strides in aerospace engineering, especially in conquering the complexities of re-entry. As a spacecraft re-enters, the immense energy expended in escaping Earth's gravitational pull and achieving orbit is

dissipated through intense heat. This entails the use of a re-entry vehicle tasked with skillfully navigating through Earth's atmosphere, facing high velocities that trigger the formation of a bow shock ahead of the vehicle and heightened aerodynamic heating. Tackling these hurdles is paramount to ensuring the safe and reliable return of astronauts and cargo.

The re-entry into the earth's atmosphere occurs at very high velocities corresponding to flight Mach numbers of 30 or even more. These hypersonic flight conditions are associated with several difficult

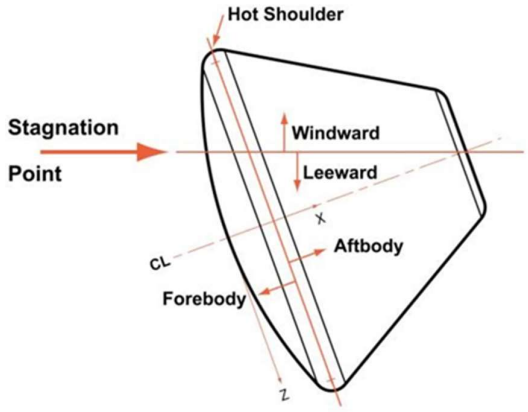

Fig 1. Key design features of CEV [1]

To further enhance aerodynamic heating reduction in the Crew Exploration Vehicle (CEV), an additional approach involves the implementation of a retro propulsion system. Retro propulsion, the technique of using engines to decelerate a spacecraft during descent by firing them in the opposite direction of travel, is a crucial technology for space programs and planetary entry, descent, and landing (EDL) [3]. It enables safe landings for high-mass payloads and potential human missions on various planets by altering aerodynamic characteristics at supersonic speeds. This innovative system works by displacing the bow shock wave further away from the CEV during re-entry, thereby minimizing the impact of aerodynamic heating.

The interaction between retro-propulsion flow and high-speed free-stream flow significantly impacts the heat flux experienced by entry vehicles, especially in hypersonic flow environments [4][5]. This heat flux is influenced by the establishment of a supersonic shear layer along the outer jet boundary, driven by large velocity differences between the subsonic flow behind the bow shock and the opposing supersonic jet flow.

2. COMPUTATIONAL METHODOLOGY

The research is based on a re-entry vehicle design adapted from the Orion Crew Exploration Vehicle. Key design features are outlined in Fig 1, and the vehicle dimensions are provided in Fig 2. The revised crew module design integrates a nozzle in its forebody, designed to accommodate two distinct Mach velocities: Mach 2 and Mach 4. The nozzle design process standardized the nozzle exit diameter at 0.1 meters. The area-Mach number relations were used to calculate the inlet diameter and area ratio for each of the nozzle designs.

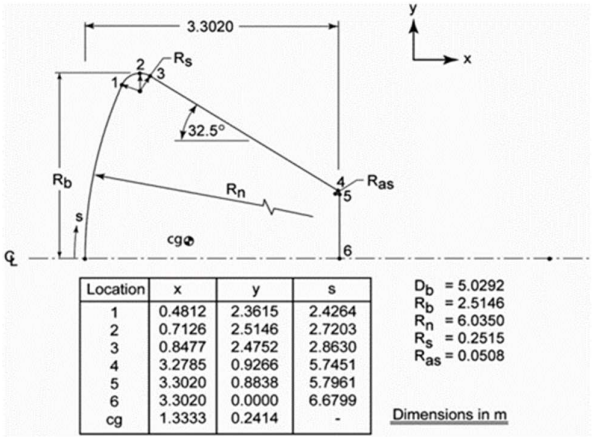

Location	x	y	s
1	0.4812	2.3615	2.4264
2	0.7126	2.5146	2.7203
3	0.8477	2.4752	2.8630
4	3.2785	0.9266	5.7451
5	3.3020	0.8838	5.7961
6	3.3020	0.0000	6.6799
cg	1.3333	0.2414	-

Fig. 2 CEV Dimensions [5]

The structured mesh was created for the baseline model and two modified models for two different exit Mach numbers. Detailed views of the nozzle mesh for different Mach numbers can be seen in Fig.4 and Fig.5. The meshing process was performed using ANSYS Fluent (CGNS format), and subsequently converted to CFD++ format using Pointwise software.

The computational simulations employed the 3D, implicit density-based AUSM+ solver of flux type for all calculations. The Reynolds Averaged Navier Stokes (RANS) equations were solved. To close the RANS equations, the two-equation k-Ɛ turbulence model was selected as it predicts separation and reattachment with greater accuracy than other models. The turbulence intensity was maintained at
0.02. Viscosity was defined using Sutherland's viscosity law. The discretization scheme remained

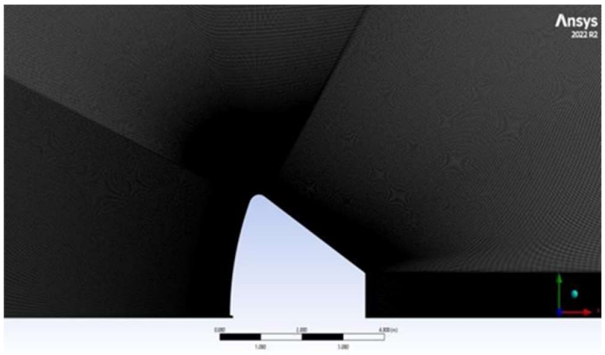

Fig. 3 Computational domain
set to a second-order upwind scheme throughout the iterative process.

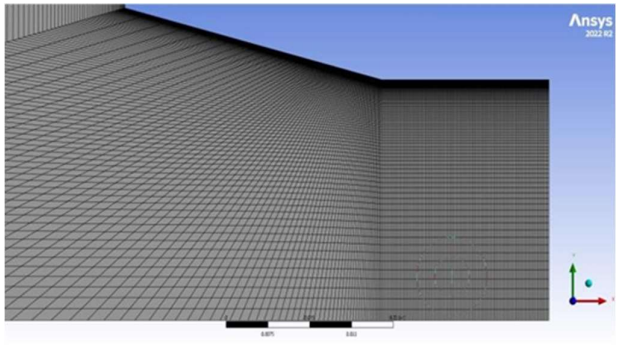

Fig. 4 Mesh of nozzle for Mach number 2

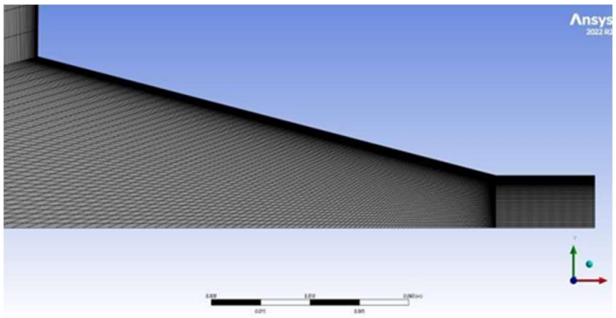

Fig. 5 Mesh of nozzle for Mach number 4

Based on earlier studies, Table 1 presents the freestream boundary conditions.

Table 1. Freestream boundary conditions

FREESTREAM PROPERTY	VALUE
Pressure (N/m^2)	42.5
Temperature (K)	252.7
Velocity (m/s)	6721

3. RESULTS AND DISCUSSION

The flow field around the Orion CEV is initialized to free stream values all over the domain. As the flow simulation starts the bow shock and the boundary layer on the vehicle are formed. The 2D flow field solution for the Orion CEV fixed at zero angle of attack is discussed.

3.1 Baseline CEV model

3.1.1 Mach number

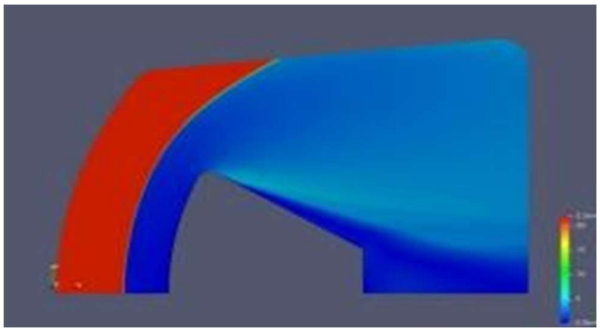

Fig. 6 Mach number contour of baseline CEV model

Fig. 6 shows Mach number flow contour for the crew module at a Mach number of 21. A detached bow shock is formed in front of the crew module due to bonding between the incoming and reflected atmospheric molecules. As the hypersonic flow encounters the bow shock, it undergoes compression, leading to reduction in velocity and Mach number. Also shows the rapid increase in aerodynamic heating due the bow shock formation. The bow shock wave act as a barrier, slowing down the incoming airflow and creating a region of very high pressure and temperature.

3.1.2 Temperature

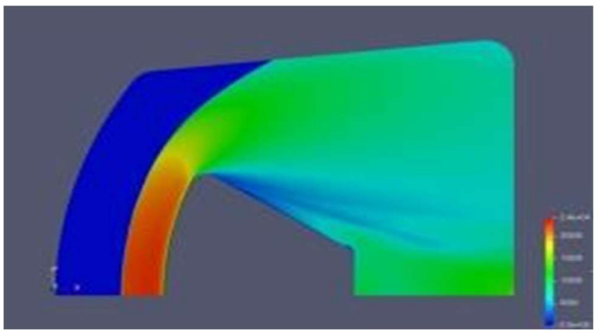

Fig. 7 Temperature contour of baseline CEV model

Fig. 7 shows temperature contour of baseline CEV model, the increase in temperature across the bow shock wave. The temperature rises from the free stream value of 252.7 K to 23,000 K downstream of the shock.

3.1.3 Cp variation

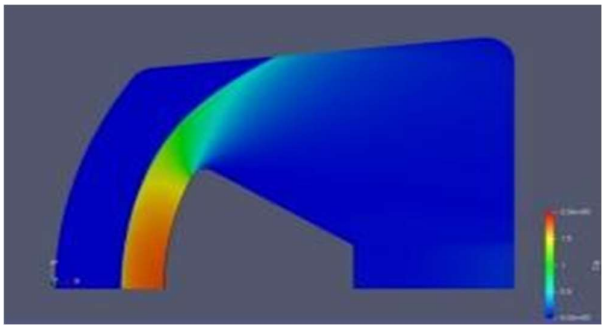

Fig. 8 Cp variation contour of baseline CEV model Fig. 8 shows the pressure coefficient variation

across the bow shock wave. Upstream of the shock, Cp values are generally lower, corresponding to the lower pressure associated with higher velocities in the free stream.

Moving downstream of the shock, Cp values increase, reflecting the compression effects induced by the bow shock.

3.2 Comparison of the modified CEV models

3.2.1 Mach number

Fig. 9(a) shows a retro-propulsion system fixed on the forebody of the CEV model. This propulsion system discharges a supersonic jet through a Mach 2 nozzle towards the downstream region of the bow shock wave. The nozzle flow, characterized by its Mach 2 speed, undergoes an interaction with the hypersonic freestream as it opposes the bow shock wave. A barrel shock is formed when the flow is expanded through the nozzle, showing that the nozzle is under expanded. Fig. 9(b) shows the detailed view of the jet shock interaction. The nozzle itself is described as under-expanded because the pressure at the nozzle outlet is higher than the pressure downstream of the shock wave. This pressure difference causes the nozzle flow to expand rapidly upon exiting the nozzle, leading to the formation of a barrel shock downstream.

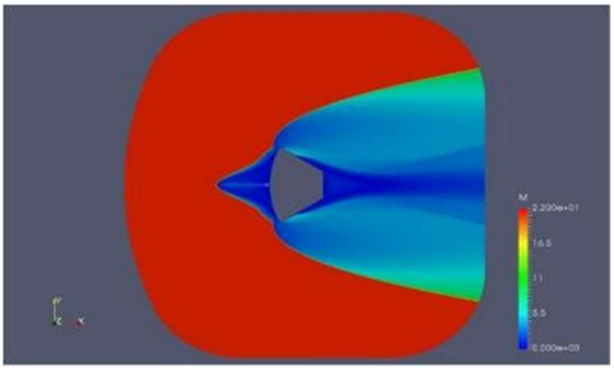

Fig. 9(a) Mach number contour of modified CEV model with exit Mach number 2 nozzle

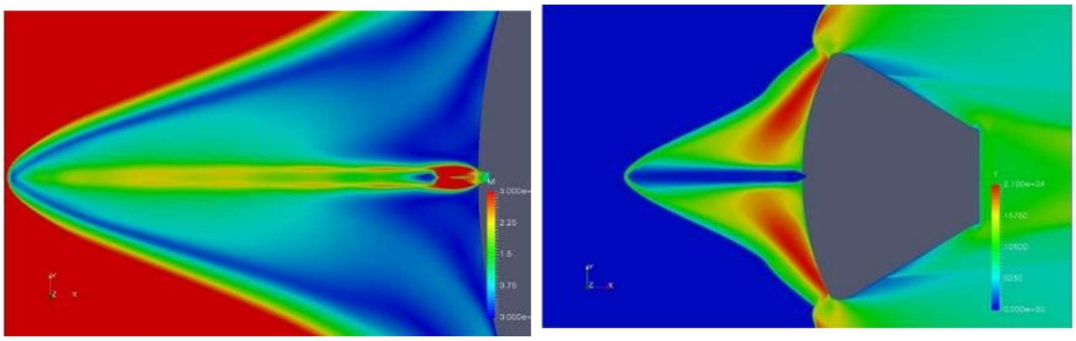

Fig. 9(b) Rescaled Mach number contour

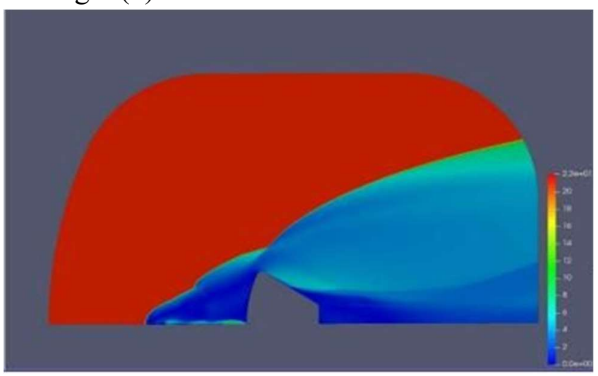

Fig. 9(c) Mach number contour of modified CEV model with exit Mach number 4 nozzle

Fig. 9(c) shows Mach number contour of modified CEV model with exit Mach number 4 nozzle, the Mach number variations resulting from the firing of a retro-propulsion variations resulting from the firing of a retro-propulsion nozzle. In this case, the jet is expanded through a Mach 4 nozzle instead of Mach 2, as previously described. Notably, the retro-propulsion has a pronounced effect as the bow shock wave is entirely displaced away from the re-entry vehicle. This displacement significantly reduces the impact of the bow shock wave on the CEV blunt body surface, leading to a distinct change in the Mach number pattern.

3.2.2 Temperature

Fig. 10(a) shows the temperature changes associated with firing a nozzle jet, resulting in the displacement of the bow shock wave far from the crew module or re-entry vehicle. This displacement has a mitigating effect on the heat experienced by the CEV model. Specifically, the temperature decreases from 23,000K to 21,000K compared to the configuration without the jet.

Fig. 10(b) shows the temperature contour of modified CEV model with a Mach 4 nozzle at center

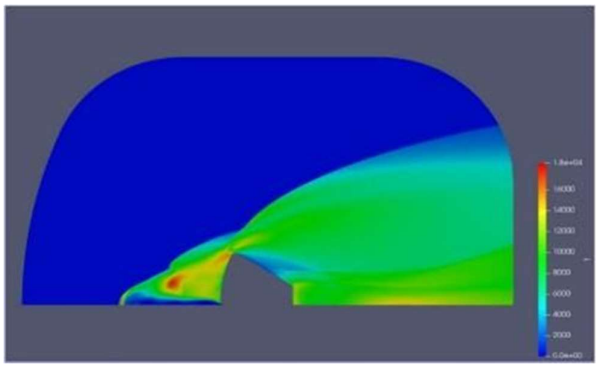

Fig. 10(a) Temperature contour of modified CEV model with exit Mach number 2 nozzle

Fig. 10(b) Temperature contour of modified CEV model with exit Mach number 4 nozzle

of its forebody reveals significant changes compared with a Mach 2 nozzle. Notably, the bow shock is visibly displaced further away from the vehicle in the Mach 4 nozzle setup. This displacement has a substantial impact on the temperature distribution, effectively reducing the temperature effects associated with the detached bow shock wave. In the absence of the jet configuration, the peak temperature reaches 23,000K. However, with the displacement of the bow shock caused by the Mach 4 nozzle, the peak temperature corresponds to a decrease in heat flux affecting the vehicle's body, indicating the effectiveness of the Mach 4 nozzle in mitigating the thermal impact during re-entry into atmosphere.

3.2.3 Cp variation

From fig. 11(a), we can see that there is a recirculation area both above and below the jet, contributing to elevated temperatures and pressure coefficients (Cp) near the shoulder regions of the CEV model. It is worth noting that the bow shock wave is not entirely shifted away from the vehicle's body, instead, it remains closer, particularly in the shoulder regions.

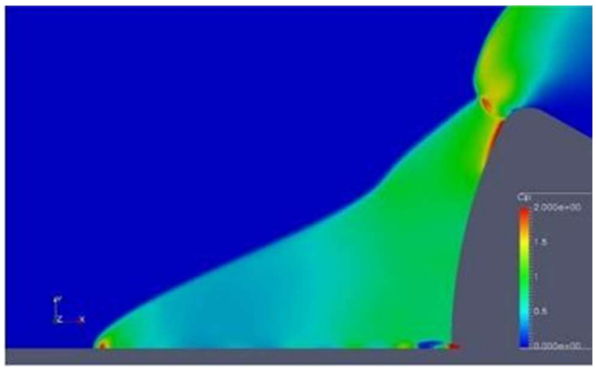

Fig. 11(a) Cp variation contour of modified CEV model with exit Mach number 2 nozzle

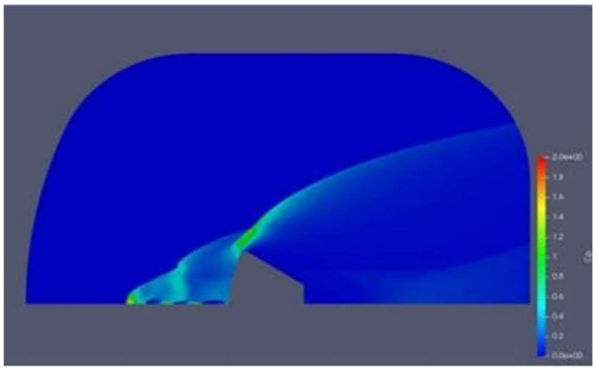

Fig. 11(b) Cp variation contour of modified CEV model with exit Mach number 4 nozzle

Fig.11 (b) shows Cp contour of modified CEV model with a Mach 4 nozzle, Cp variation resulting from firing of retro propulsion through Mach 4 nozzle. The intricate process of forming a series of barrel shocks in under expanded supersonic jets involves the interaction of high-pressure jet flow with the surrounding ambient environment. Emerging from an under expanded nozzle with a pressure exceeding that of the ambient surroundings, the supersonic flow transforms into a high-velocity jet with elevated pressure. As this high-pressure jet expands radially into the lower-pressure ambient environment, encountering a pressure gradient induces deceleration. Radial expansion begets the formation of expansion waves, which interact with compression waves generated by the supersonic flow, ultimately leading to the creation of shock waves. The first barrel shock wave materializes as a result, demarcating the boundary between the high-pressure jet flow and the lower-pressure ambient environment. Downstream propagation prompts the reflection and refraction of the shock wave off the ambient environment, giving rise to a series of barrel shocks at various radial positions within the jet. This sequence creates a characteristic shock-wave structure, characterized by alternating regions of high and low pressure.

4. CONCLUSIONS

The retro-propulsion system is examined, leading to the bow shock wave being displaced significantly from the CEV. This displacement is due to firing of the nozzle jet. Compared to the baseline CEV model, the temperature at the forebody of the CEV decreases from 23,000K to 21,000K. Furthermore, when the Mach 4 nozzle jet is utilized, the heating near the forebody drops further to 17,000K. It is observed that the Mach 4 nozzle displaces the bow shock wave

further from the CEV compared to the Mach 2 nozzle jet. This is because, when using the Mach 2 nozzle jet, the bow shock wave is not fully replaced from the CEV's forebody. Conversely, the Mach 4 nozzle jet completely replaces the bow shock wave from the CEV's forebody. Ultimately, the comparison demonstrates that the Mach 4 nozzle jet is more effective in reducing aerothermal heating than the Mach 2 nozzle jet. This study reveals that using a retro-propulsion system can effectively diminish the aerothermal heating experienced during re-entry into the Earth's atmosphere. For future investigations, it may be beneficial to explore configurations that employ multiple nozzle jets distributed across the forebody, or angled nozzle jet designs. Additionally, varying the positioning of the nozzle jet within the forebody, as opposed to its central placement, could be explored.

ACKNOWLEDGEMENT

This research has been made possible with the generous support from the Vikram Sarabhai Space Centre (VSSC), a premier research institution under the Indian Space Research Organisation (ISRO). I express my sincere gratitude to the CFDD team of VSSC for their invaluable guidance, resources, and assistance, which have contributed significantly to the completion of this work.

REFERENCES

[1] Shafeeque. (2017). CFD analysis on an atmospheric re-entry module. International Research Journal of Engineering and Technology, 04(01).

[2] Berry, S. A., Horvath, T. J., Lillard, R. P., Kirk, B. S., & Fischer-Cassady, A. (2009). Aerothermal testing for Project Orion Crew Exploration vehicle. 41st AIAA Thermophysics Conference. https://doi.org/10.2514/6.2009-3842

[3] Korzun, A. M., Braun, R. D., & Cruz, J. R. (2009). Survey of supersonic retropropulsion technology for Mars entry, descent, and landing. Journal of Spacecraft and Rockets, 46(5), 929–937. https://doi.org/10.2514/1.41161

[4] Lee, S., & Park, G. (2019). Retro-Jet experimental study for reusable rockets in a hypersonic flow. European Conference for AeroSpace Sciences, 598. http://koasas.kaist.ac.kr/handle/10203/263365

[5] Votta, R., Schettino, A., Ranuzzi, G., & Borrelli,
S. (2009). Hypersonic Low-Density aerothermodynamics of Orion-Like exploration vehicle. Journal of Spacecraft and Rockets, 46(4), 781–787. https://doi.org/10.2514/1.42663

[6] Bibb, K. L., Brauckmann, G. J., Walker, E. L., & Robinson, P. (2011). Development of the Orion Crew Module Static Aerodynamic Database, Part I: Hypersonic. 29th AIAA Applied Aerodynamics Conference. https://doi.org/10.2514/6.2011-3506

[7] Chanetz, B., Benay, R., Bousquet, J., Bur, R., Pot, T., Grasso, F., & Moss, J. N. (1998). Experimental and numerical study of the laminar separation in hypersonic flow. Aerospace Science and Technology, 2(3), 205–218. https://doi.org/10.1016/s1270-9638(98)80054-0

[8] Finson, M. L., & Wu, P. (1979). Analysis of rough wall turbulent heating with application to blunted flight vehicles. 17th Aerospace Sciences Meeting. https://doi.org/10.2514/6.1979-8

[9] Govindan, S., & Nair, P. (2018). Effect of numerics and laminar-turbulent transition on heat flux distribution simulation over a typical re-entry module. Applied Thermal Engineering, 131, 849– 863.
https://doi.org/10.1016/j.applthermaleng.2017.12.03 3
[10] Kinney, D. J. (2009). Development of the ORION crew exploration vehicle's aerothermal database using a combination of high fidelity CFD and engineering level methods. 47th AIAA Aerospace Sciences Meeting Including the New Horizons Forum and Aerospace Exposition. https://doi.org/10.2514/6.2009-1100
[11] Lees, L. (2003). Hypersonic flow. Journal of Spacecraft and Rockets, 40(5), 700–735. https://doi.org/10.2514/2.6897
[12] Mehta, R.. (2008). Computations of flow field over Apollo and OREX reentry modules at high speed. Indian Journal of Engineering and Materials Sciences, 15, 459-466
[11] Moss, J. N., Greene, F. A., & Boyles, K. A. (2006). Orion aerodynamics for hypersonic free molecular to continuum conditions. 14th AIAA/AHI Space Planes and Hypersonic Systems and Technologies Conference.
https://doi.org/10.2514/6.2006-8081
[12] Murphy, K. J., Bibb, K. L., Brauckmann, G. J., Rhode, M. N., Owens, B., Chan, D. T., Walker, E. L., Bell, J. H., & Wilson, T. (2011). Orion Crew Module Aerodynamic testing. 29th AIAA Applied Aerodynamics Conference. https://doi.org/10.2514/6.2011-3502
[13] Patel, R. K., & Venkatasubbaiah, K. (2015). Numerical simulation of the Orion CEV reentry vehicle. Journal of Aerospace Engineering, 28(2). https://doi.org/10.1061/(asce)as.1943- 5525.0000397
[14] Rathnavel, S., Balaji, K., Prem, P. K., Sathesh,
N. R., & Vijaya, K. S. (2020). Investigation of computational flow field over a re-entry capsule at high speed. FME Transactions, 48(3), 551–556. https://doi.org/10.5937/fme2003551r
[15] Schneider, S. P. (2006). Laminar-Turbulent transition on reentry capsules and planetary probes. Journal of Spacecraft and Rockets, 43(6), 1153–1173. https://doi.org/10.2514/1.22594
[16] U, Shiva & Srinivas, Garepally. (2012). Flow Simulation over Re-Entry Bodies at Supersonic & Hypersonic Speeds. International Journal of Engineering Research & Development. 2. 29-34.
[17] Votta, R., Schettino, A., Ranuzzi, G., & Borrelli,
S. (2009). Hypersonic Low-Density aerothermodynamics of Orion-Like exploration vehicle. Journal of Spacecraft and Rockets, 46(4), 781–787. https://doi.org/10.2514/1.42663
[18] Zapryagaev, V. I., Kiselev, N. A., & Gubanov, D.
A. (2018). Shock-Wave structure of supersonic jet flows. Aerospace, 5(2), 60. https://doi.org/10.3390/aerospace5020060
[19] Votta, R., Schettino, A., & Bonfiglioli, A. (2013). Hypersonic high altitude aerothermodynamics of a space re-entry vehicle. Aerospace Science and Technology, 25(1), 253–265. https://doi.org/10.1016/j.ast.2012.02.001
[20] Zapryagaev, V. I., Kiselev, N. A., & Gubanov, D.
A. (2018). Shock-Wave structure of supersonic jet flows. Aerospace, 5(2), 60. https://doi.org/10.3390/aerospace5020060